Journal of Molecular Spectroscopy 322 (2016) 1–8

Contents lists available at ScienceDirect

Journal of Molecular Spectroscopy

journal homepage: www.elsevier.com/locate/jms

Rao Prize article

Infrared emission spectroscopy of atmospheric-pressure ball plasmoids ☆

Scott E. Dubowsky [a], Bradley Deutsch [b], Rohit Bhargava [b], Benjamin J. McCall [c,*]

[a] Department of Chemistry, University of Illinois, Urbana, IL 61801, USA
[b] Department of Chemical and Biomolecular Engineering, University of Illinois, Urbana, IL 61801, USA
[c] Departments of Chemistry and Astronomy, University of Illinois, Urbana, IL 61801, USA

ARTICLE INFO

Article history:
Received 29 September 2015
In revised form 30 January 2016
Accepted 5 February 2016
Available online 9 February 2016

Keywords:
Plasmoid
Plasma diagnostics
Rotational temperature
Infrared emission spectroscopy PGOPHER
Ball lightning

ABSTRACT

We report the first (to our knowledge) infrared emission spectra collected from water-based laboratory ball plasmoid discharges. A "ball plasmoid" results from a unique type of pulsed DC plasma discharge in which a sphere of plasma is seen to grow and eventually separate from a central electrode and last for a few hundred milliseconds without an external power source before dissipating. Typical recombination rates for plasmas at ambient conditions are on the order of a millisecond or less, however ball plasmoids have been observed to last a few hundred milliseconds, and there is no explanation in the literature that fully accounts for this large discrepancy in lifetime. The spectra are dominated by emission from water and from hydroxyl radical; PGOPHER was used to fit the experimental spectra to extract rotational temperatures for these molecules. The temperatures of the bending and stretching modes of H_2O were determined to be 1900 ± 300 K and 2400 ± 400 K, respectively and the rotational temperature of OH was found to be 9200 ± 1500 K.

1. Introduction

Low-temperature and atmospheric-pressure plasmas have developed as essential tools across several industries over the past few decades. The tunability of plasma discharge parameters allows for the selection of chemically and physically reactive components of the ionized medium, and operating a discharge at ambient pressures fosters numerous applications of plasmas in different settings. For example, the electron density and temperature, identities and number densities of reactive ions and radicals, UV photon flux, and flow rate of gases can all be tuned and optimized for interactions with different surfaces ranging from plastics to human teeth to the top layers of the skin. There has been much development of plasmas as tools for semiconductor processing [1,2], medicine [3–5], dentistry [6], air purification [7], wastewater [8] and biomedical [9–13] sterilization, as agents for controlled mutagenesis [14], and in the food processing and sterilization industry [15,16]. Additionally, ambient plasmas are attractive as soft ionization sources for mass spectrometry [17–19], especially due to the much less complicated sample preparation required for ambient ionization using plasmas.

Plasmas that are self-sustaining and have a definitive shape but are not confined between two electrodes or any external fields are referred to as plasmoids. A several-kilovolt capacitive discharge above the surface of a weak electrolyte can be used to generate water-based plasmoids [20] which take the form of a sphere, thus this particular type of discharge is referred to as a "ball" plasmoid discharge. In contrast to other direct-current (DC) plasma discharges (arc, corona, glow, dielectric barrier) [21], ball plasmoid discharges are generated by intentionally designing the electrodes such that a tremendous pulse of current causes a plasma to form at the tip of the cathode, above the surface of the electrolyte [20,22–24]. While still forming, the plasma grows, rises, and eventually separates from the cathode and can be seen as a distinct sphere of plasma for an extended period of time. The discharge occurs in three phases (Fig. 1): the pre-initiation, buildup, and detachment phases [25,26]; it is perhaps the detachment portion of the discharge, when an autonomous plasmoid can be observed, that is the most interesting. Plasma discharges at ambient pressures are not expected to last for more than a millisecond without an external power source [27,28], however ball plasmoids emit light for approximately 200 ms even when no current flows between the electrodes.

☆ The article is based upon a presentation by the author at the 70th International Symposium on Molecular Spectroscopy in June 2015 at Urbana-Champaign, which was selected by the Symposium Prize Committee for the Rao Prize as one of the three best presentations by a graduate student.

* Corresponding author.
E-mail address: bjmccall@illinois.edu (B.J. McCall).

http://dx.doi.org/10.1016/j.jms.2016.02.005
0022-2852/

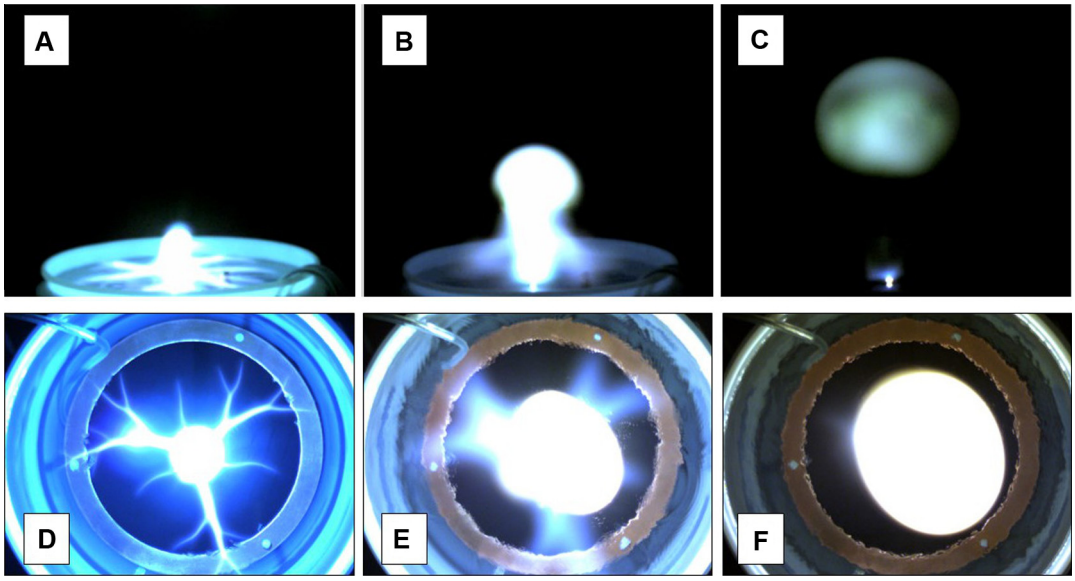

Fig. 1. Images obtained from high-speed videography of plasmoid discharges. (A–C): initiation, propagation, and detachment phases of the discharge. (D–F): top-down view of the same phases shown in A–C, taken from an identical discharge on the same day.

Recently, several groups have begun to characterize ball plasmoid discharges in attempts both to explain the long lifetime of the plasmoid and to study the mechanism of ball plasmoid formation [23,24,29,25,26], and this collection of papers has provided a foundation for more detailed studies of the system. Our goal for the experiments described in this article is twofold: to expand the emission spectroscopy performed by Versteegh et al. [23] into the infrared, and to confirm the molecular assignments obtained from infrared absorption spectroscopy presented by Friday et al. [29]. In addition to identifying the molecules which are emitting in the infrared, we aim to determine rotational temperatures for each of the emitting molecules, which will provide a more complete picture of the energy distribution of products generated during plasmoid formation and will also allow for an approximation of the gas-kinetic temperature of the plasmoid to be made.

Ball plasmoids are considered to be laboratory analogues of ball lightning, a puzzling and currently unexplained natural phenomenon which was only recently observed in the field with scientific instrumentation [30]. Although rare, there are numerous reports available in the literature describing a luminous sphere of light dancing through the sky, sometimes lasting tens of seconds before dissipating. Some reports describe a quiet fizzling out of the light, but others indicate that the ball leaves destruction in its wake as it disappears with tremendous energy. There is also debate in the literature over the theories describing the formation and other properties of ball lightning [31–35], often with little or no experimental evidence, therefore there is currently no explanation (or set of explanations) as to why ball lightning behaves in these mysterious ways.

2. Experimental

2.1. Plasmoid discharge source

The equipment and electronics that we use to generate plasmoid discharges have been described previously [29,26], however some changes have been made to the circuitry to better control and monitor the discharge. To provide as accurate a description of the apparatus as possible, the key components of the system will be described. The next paragraph describes the general process by which ball plasmoids are generated, and the following paragraphs describe additional components of the system. As is always the issue with performing these measurements, there is a high shot-to-shot variability in successive plasmoid discharges. Much in the same way that no two lightning strikes are alike, identical conditions can produce plasmoid discharges with different underlying characteristics (size, lifetime, amperage, rise velocity, etc.).

The electrode setup is contained within a store-bought five-gallon polypropylene bucket which is filled with deionized water. The conductivity of the water is adjusted using concentrated HCl. Conductivity measurements are taken with a hand-held, waterproof meter (Oakton PCSTest™35). The cathode is positioned such that just the tip of the electrode protrudes above the surface of the water approximately 1–2 mm. The cathode which is used in all of the following experiments is a solid tungsten rod with a diameter of 6 mm. The cathode is insulated from the electrolyte using a tube of alumina with an inner diameter of 6 mm and an outer diameter of 8 mm. No metal ions from the cathode were desired to be present in the discharge during these experiments, so tungsten was chosen for its high durability and resistance to sputtering and spalling. This cathode was chosen in order to minimize ion-neutral and ion–electron interactions caused solely by electrode materials, thus producing a plasmoid from only molecules in the air and molecules just above the surface of the electrolyte [26]. A copper ring is used as the anode and is positioned perpendicular to the orientation of the cathode, in other words the plane of the anode is parallel to the surface of the electrolyte. This entire electrode is submerged in the weakly conductive aqueous solution with a final depth of approximately 12 cm below the surface of the electrolyte.

Fig. 2 provides an illustration of the circuitry used in our laboratory. A Glassman EK Series high-voltage DC power supply is used to charge large parallel-plate, oil-filled capacitors (Maxwell) to 1–10 kV. The capacitors can be used individually or can be wired in parallel to generate capacitances up to two milliFarads. Three Ross Engineering E Series high-voltage relays are used to make connections that will charge the system, send current pulses to the discharge container, or ground the system. An Arduino®Uno microcontroller board controls the timing of these switches, and the same microcontroller is used to record voltage and current measurements via a voltage divider and Hall effect sensor, respectively. High-speed videography is performed with a Pixelink®PL-

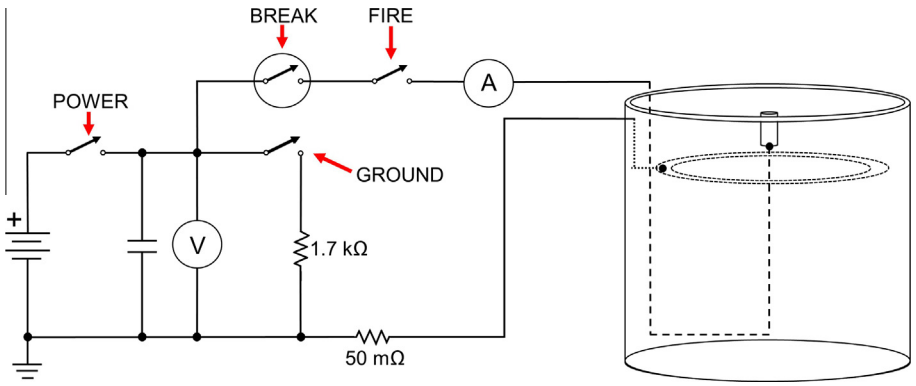

Fig. 2. A simplified circuit diagram of the plasmoid discharge circuit. The "POWER" relay delivers current to the capacitor bank, the "FIRE" relay delivers the pulse to the electrodes, "BREAK" is the vacuum relay which breaks current to the electrodes, and finally the "GROUND" relay grounds the system. V and A are a voltage divider and a Hall effect current sensor, respectively.

B&42U camera with a frame rate of 98 fps. Discharge parameters are chosen based both on the geometry of the setup and an optimization of safety to personnel and equipment, therefore no discharges above 7 kV are ever performed due to physical limitations of the equipment (temperature rating of power resistors, arcing concerns, etc.). Future additions and improvement to the circuitry will allow for larger voltages and capacitances to be used safely and successfully.

The parameters of the discharges described in this article are the following: the capacitor (873 μF) was charged to 6 kV, the conductivity of the electrolyte was set to 320 μSiemen, and the tip of the cathode was set flush to the tip of the alumina insulator which was positioned to protrude approx. 1–2 mm above the surface of the electrolyte. The conductivity of the electrolyte did not change significantly between experiments due to resistive heating. All spectra were recorded on the same day, under identical conditions.

2.2. Spectroscopic measurements

Infrared emission spectroscopy was performed using a Bruker VERTEX 70 Fourier-transform infrared spectrometer in a double-pass configuration at 4 cm^{-1} resolution and a (mirror) scan rate of 40 kHz. Spectra were collected between 1000 and 5000 cm^{-1}. The time-domain interferogram data from the spectrometer were high-pass filtered using a second-order Butterworth filter, Hanning apodized, and Hilbert transformed (phase correction) to generate emission spectra. The lineshapes in these spectra are ultimately dictated by the response function of the instrument (a Hanning function Fourier transformed to a *sinc* function in this case), thus the experimental lineshapes are best described by a Lorentzian profile with a FWHM of 4 cm^{-1}. Only one scan was used for each measurement, and it is important to note that the spectrometer and discharge electronics (each with their own small internal triggering delays) were triggered by hand. The spectrometer and discharge were triggered independently by two individuals after a countdown; no time-resolved measurements could be performed using this setup.

Fig. 3 provides a birds-eye view of the experimental setup. The HeNe laser within the instrument was used in conjunction with additional optics placed outside of the instrument to align the light emitted from the plasmoid into the spectrometer. To confirm the placement of the optics, a flame from a butane lighter was held where the plasmoid would be discharged and at points along which the emitted light was presumed to be traveling. The intensity counts on the detector were monitored in real time as the flame was brought in and out of the optical path. The intensity counts at the detector would increase by a few orders of magnitude when emitted light from the flame was detected. An opaque sheet was also placed between the plasmoid and the optics to isolate the emitted light. A hole was cut into the sheet such that the tip of the electrode was masked but the plasmoid itself was not. This eliminated the possibility of light from the hot cathode interfering with our measurements. This also minimized reflections off of other surfaces in the laboratory.

3. Results and discussion

3.1. Emission spectra

Fig. 4 shows several spectra that were obtained over the course of the experiment. A cursory examination of these data shows that water dominates the spectra, but a closer inspection shows that emission from hydroxyl radical is also present. Using the HITRAN [36] database in conjunction with the PGOPHER [37] program, a simulated mixture of these molecules was generated and compared to the experimental spectra. The simulated spectrum displayed in Fig. 4 (the uppermost spectrum) shows good agreement with the experiment in terms of the molecules that are emitting from the plasmoid.

Given that there was a significant pathlength between the plasmoid and the spectrometer in these experiments, it was necessary to account for absorption by water and CO_2 along this optical path. In order to address this issue, the observed spectra were divided by an absorbance spectrum of CO_2 and water (298 K, 2.06 m pathlength, Lorentzian lineshape; 4 cm^{-1} linewidth, 1 atm) generated using HITRAN online (http://hitran.iao.ru/). In each spectrum this resulted in a significant increase in emission signal in the regions where atmospheric CO_2 and water readily self-absorb, however there is little effect on the intensity between 2400 and 3200 cm^{-1} (where emission from OH is present). The corrected spectra used in fitting can be found in the supplementary material.

As would be expected, the difficulties associated with obtaining a spectrum after triggering the discharge resulted in missing the emission from the plasmoid in some cases. Some of the spectra exhibited only a broad and featureless continuum spanning approximately 2000 cm^{-1}; these spectra were rejected as unusable. Furthermore, there were trials in which we thought that emission from the plasmoid was collected by the instrument, however only instrumental noise was observed in the spectra, which speaks to the importance of triggering the discharge and spectrometer simultaneously.

3.2. Fitting

The PGOPHER [37] program was used to fit the corrected spectra to simulated spectra of water and hydroxyl radical. At the outset of our rotational analysis we attempted to fit a mixture of both

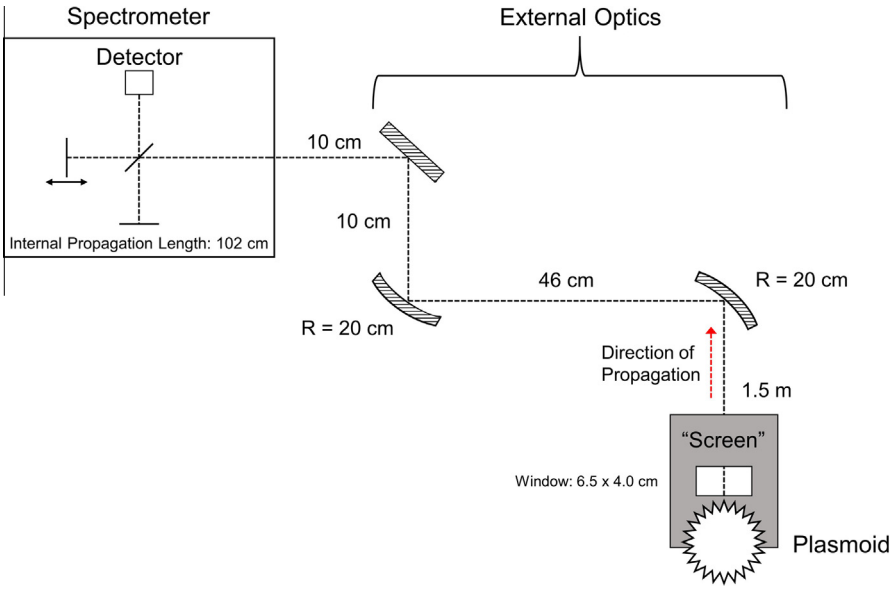

Fig. 3. Bird's eye view of optical setup for experiment. Relevant distances and focal lengths are provided (not to scale).

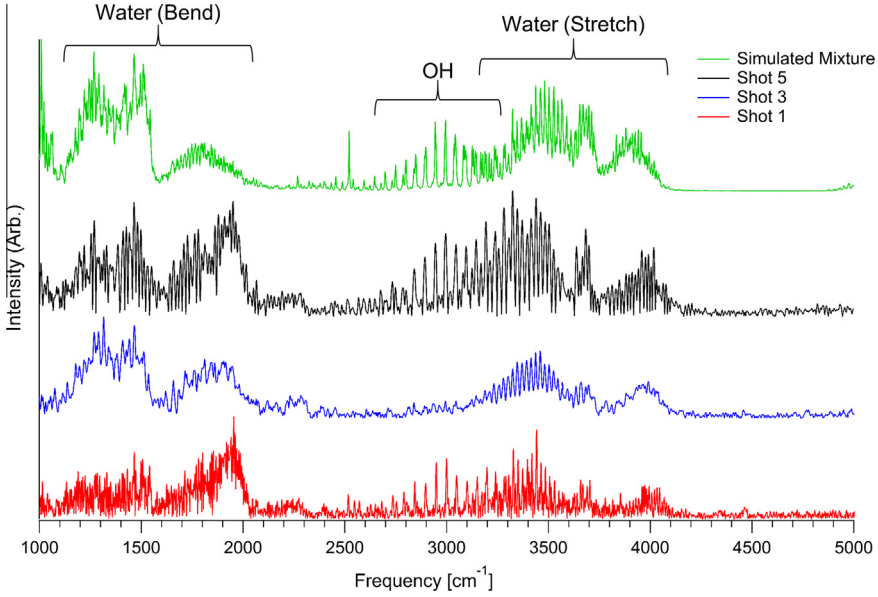

Fig. 4. Upper curve: simulated spectrum of a mixture of H_2O and OH. Lower curves: three examples of emission spectra collected from ball plasmoid discharges, offset for clarity. Spectra were obtained under identical conditions.

of these molecules to the experimental data, however PGOPHER's functionality allows for only a single rotational temperature to be floated during fitting. We expected the temperatures of different plasmoid constituent molecules to be rather different from one another, therefore, each molecule was fit separately. Furthermore, vibrational excitation (and relaxation) occurs differently for each degree of freedom in nonequilibrium air discharges, thus the three vibrational modes of water are also expected to have slightly different values of rotational temperature. The generic fitting procedure involved generating a spectrum of the molecule of interest using the HITRAN line list (imported directly into PGOPHER), modifying the simulation to reflect emission data as per Western's [37] suggestions, overlaying an experimental spectrum in the software, adjusting the scale of the experimental spectra, and finally floating the value for rotational temperature until the fit converged.

When first fitting the data to a spectrum of water we noticed that the fits would converge on a rotational temperature, however some of the residuals appeared to be the result of an unphysical fit. Indeed, when good results were returned from fits to the stretching modes, fits to the bending mode were poor. To resolve this issue, the stretching modes and bending mode of water were analyzed independently; the symmetric and asymmetric stretching modes were fit together, but the bending mode was fit separately. As a result of significant hot band emission, the emission profile of the bending mode was not fully reproduced by the PGOPHER simulations (although hot bands were included in the simulations), resulting in fits taking longer to converge. Fits were performed between 3200–4300 cm^{-1} and 1000–2500 cm^{-1} for the stretching modes and bending mode, respectively (see supplemental material). Numerical results from each of the fits to H_2O are shown in Table 1, and an example of a complete fit is provided in Fig. 5.

Table 1
Calculated rotational temperatures for the vibrational bands of water.

Shot	$T_{rot}^{stretch}$ [K]	T_{rot}^{bend} [K]
1	2300	2000
2	3300	1800
3	1700	2400
4	2200	1400
5	2300	1700
Average	2400 ± 400	1900 ± 300

The rotational temperatures we report show the extent of molecular excitation in the discharge and are comparable to those obtained from the emission of water in oxy-acetylene flames [38].

A similar procedure was used to determine the rotational temperature of hydroxyl radical. The spectra were fit from 2800 to 3200 cm^{-1}, again holding the Lorentzian linewidth constant at 4 cm^{-1}. An example of a fit to OH is shown in Fig. 6, and numerical results of the fits are presented in Table 2. In one particular instance (Shot 3, shown in Fig. 4), the intensity of the signals in the OH emission region were comparable to the noise floor, which resulted in the fits not converging on a rotational temperature. Therefore the values we report for hydroxyl radical are obtained from four separate spectra rather than five. The average rotational temperature of OH was found to be 9200 K, which is high for ambient plasmas. This value is however lower than what has previously been reported for this system [23]; the measurements reported herein were most likely made later in the discharge when compared to those of Versteegh et al. Since the rotational temperature of each constituent molecule must rapidly decrease to room temperature over the course of the discharge, it follows that the rotational temperature would be lower when probing later in the discharge. Time-dependent measurements would be extremely beneficial for the confirmation of rotational temperatures at different stages of the discharge.

There is also an unknown source of emission in the experimental spectra between approximately 2250–2400 cm^{-1}. There are several potential molecular sources for this emission, including CO_2 and CO; the 4.3 μm band of CO_2 [39] and the vibrational band of CO [40] overlap in this region, however this signal is most likely not a result of emission from CO, as the vibrational band of CO is centered approximately 100 wavenumbers to the red of the anomalous feature. We attempted to fit the corrected spectra to a simulation of CO_2 in the same fashion described above, but fits to this molecule did not fully reproduce the shape or intensity of the observed feature, even at high temperatures (see Fig. 7). This region is further complicated by the fact that self-absorption by CO_2 readily occurs in this frequency range. Thus the identity of the cause of the signal in this region remains a mystery; however, the emission profiles shown in Fig. 7 do seem to correspond to that of CO_2 in *some* way. Friday et al. [29] present evidence which suggests that CO_2 may be present in the plasmoid as a result of electrode oxidation, but this does not refute the possibility of gaseous CO_2 emitting from plasmoids produced with a tungsten electrode. Additional measurements of discharges with less shot-to-shot variability would allow for a much more concrete understanding of emission in this region, and improved spectral resolution would allow for a more traditional Boltzmann analysis of a set of known transitions.

The average rotational temperature for OH reported here is limited by the spectral resolution and lack of a thorough Boltzmann analysis, however the procedure used to fit the data provide a reasonable estimate of the rotational temperature. The high temperatures of water and hydroxyl radical indicate that upper vibrational and rotational states of plasmoid constituent molecules are highly populated, which is expected for a nonequilibrium air plasma. These upper states could be populated directly during the discharge via vibrational/rotational excitation processes, or by chemical reactions in the plasmoid. For example, highly-excited OH radicals are thought to be generated by electron impact ionization of water molecules, while other less excited radicals could be generated by excitation of previously-formed OH via other mechanisms. A more thorough analysis of better-resolved transitions could facilitate a two or three temperature model of OH rotational

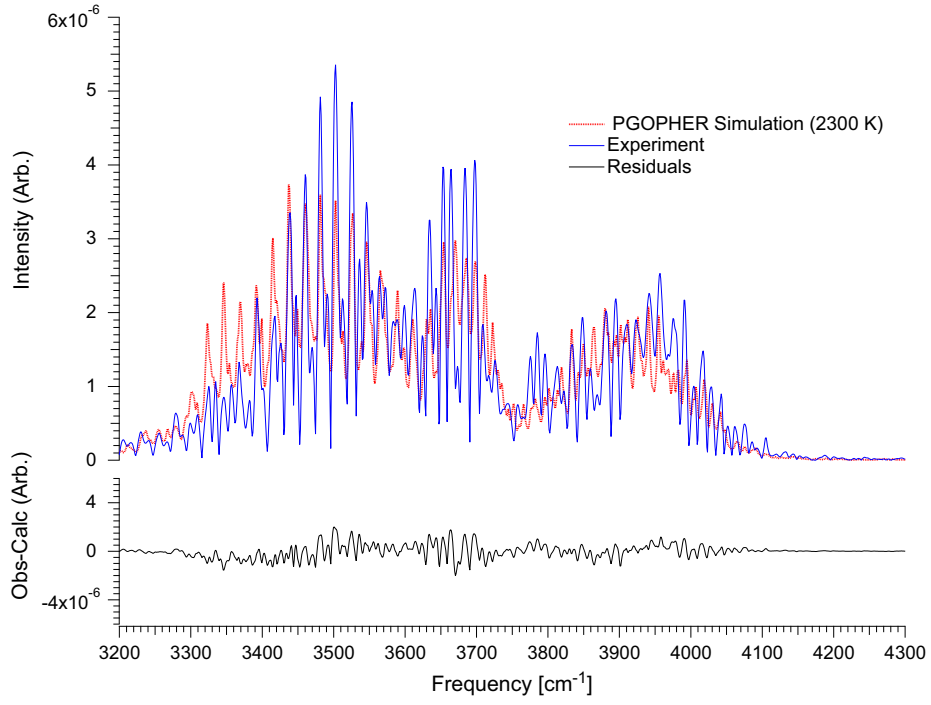

Fig. 5. Example of a fit to the stretching modes of water. This fit is to the spectrum obtained from Shot 4 (see Table 1).

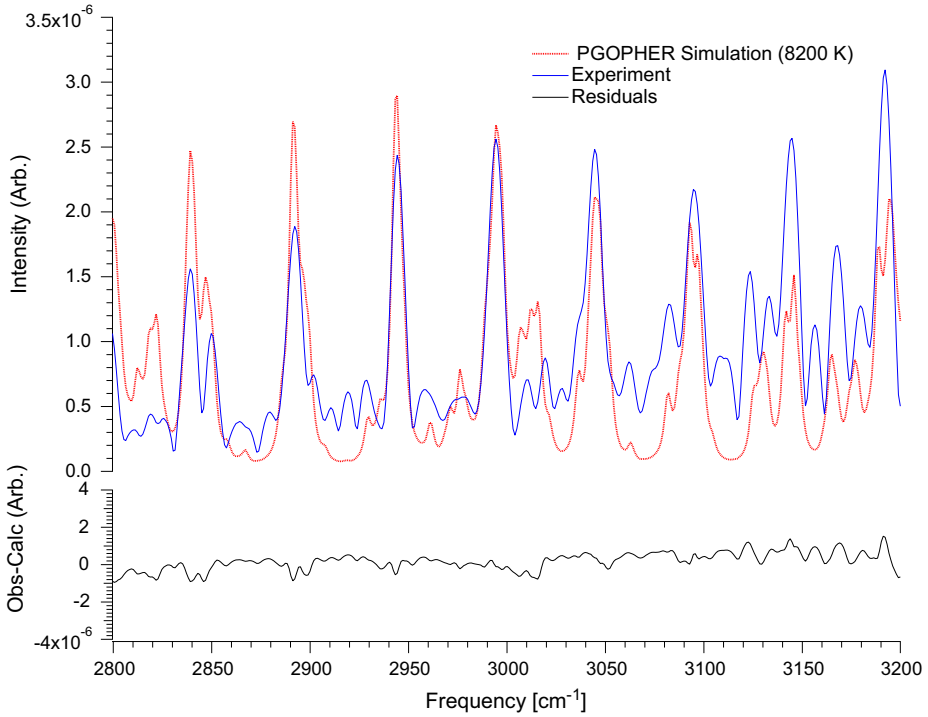

Fig. 6. Example of a fit to hydroxyl radical. This fit is to the spectrum obtained from Shot 2 (see Table 2).

Table 2
Calculated rotational temperatures for hydroxyl radical.

Shot	T_{rot}^{OH} [K]
1	7600
2	8200
3[a]	N/A
4	12,200
5	8600
Average	9200 ± 1500

[a] S/N results in fits that do not converge.

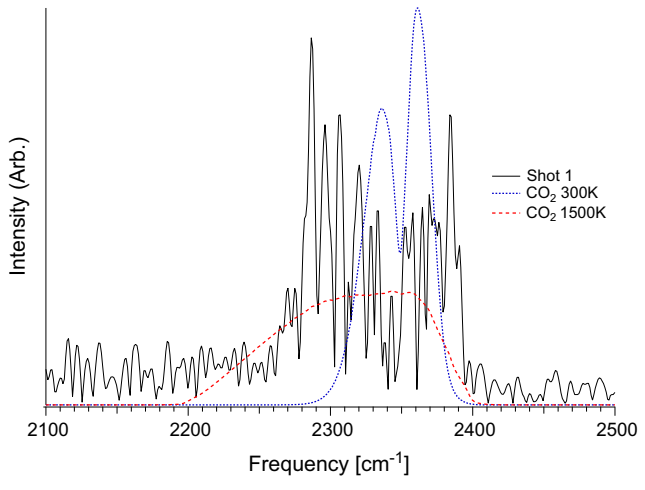

Fig. 7. Comparison of the emission profiles of CO_2 at room and high temperatures to the unexplained signal observed between 2100 and 2400 cm^{-1} in an experimental spectrum (Shot 1 in this case).

distribution, which has been studied extensively in the literature [41,42].

When comparing the spectra collected in this set of experiments to the spectrum presented by Friday et al. [29] (referred to as "the absorption spectrum" here for clarity), several differences can be noted. First, our emission spectra show signals indicative of OH from 2800 to 3200 cm^{-1}, while no evidence of OH absorption is present in the absorption spectrum. Our spectra also show high S/N for all of the vibrational modes of water, while the absorption signals corresponding to the bending mode shown in the absorption spectrum have a much smaller S/N. It is not surprising that the S/N of the bending mode is much greater in the emission spectra – it is likely that the plasmoid is highly vibrationally and rotationally excited and emission from these excited state molecules is occurring frequently. The high temperature of the plasmoid also increases the contribution from vibrational hot band transitions, which are especially prevalent in the bending mode. The two unassigned features presented in the absorption spectrum are not directly observable in our emission spectra, however this does not immediately dismiss the presence of these signals in our spectra as the observed emission profiles are incredibly complex. This complexity is further increased by the possible presence of water clusters in the plasmoid, as many of the rovibrational bands of protonated water clusters are centered within the rovibrational bands of free water molecules [43]. It is unclear at this level of spectral resolution whether emission from protonated water clusters is being detected, but this notion should not be dismissed since the protonated water dimer and trimer have been shown to be present in ball plasmoid discharges [26].

It is difficult to make a direct comparison between emission and absorption spectra collected from ball plasmoid discharges because very little is known about the optical thickness of these plasmoids. Emission spectroscopy of optically thick spheres results in collection of signals from the outermost edge of the sphere, which is not the ideal case for ball plasmoids, as plasmoids have been shown to be surrounded by an "envelope" which is cooler than the interior of the plasmoid [23]. The temperature differences between the interior and exterior of the plasmoid most likely facilitate different chemistry in the center of the plasmoid and at the air–plasmoid interface, and further study of this system with

improved spatial resolution is needed in order to study the different temperature regimes with ball plasmoid discharges.

4. Conclusion

In this work we have presented the first analysis of ball plasmoid emission in the infrared. Using a relatively simple spectroscopic setup, we were able to collect spectra that show emission from water and hydroxyl radical. These molecules are unsurprising to observe in ambient plasma discharges and have been observed in this type of discharge using absorption spectroscopy [29]. We are able to report quantitative information about the plasmoid after reducing the spectral collection time (compared to the three-second acquisition time of Friday et al.), but more importantly this analysis centered on fitting spectra which show rotational structure of constituent molecules. The rotational temperatures that were extracted from the fits of the observed spectra begin to show the energy distribution among molecules in the plasmoid and confirm the measurements of Versteegh et al., reinforcing the fact that ball plasmoid discharges are highly nonthermal and result in rapid heating and rapid cooling of constituent molecules.

In order to move this work forward experimentally and answer the ultimate question of why ball plasmoid recombination occurs much more slowly than is expected, a twofold approach is being undertaken. First, we are expanding the spectral regions in which we are probing; we are working to examine the plasmoid in the near-IR and in the UV/visible to monitor molecules such as N_2^+ and N_2^*. As the principal component of ambient air, it is highly likely that the molecular processes in which nitrogen participates are key to understanding the relaxation processes of the plasmoid. We also plan to re-examine hydroxyl radical with improved spectral and temporal resolution compared to the previous work [23]. This will facilitate a greater understanding of the energy distribution as a function of time and will also provide insight into the reactions which are (or are not) occurring during the three phases of the discharge.

Acknowledgments

We would like to thank Jui-Nung Liu (Cunningham Research Group, UIUC) for his help with operating the spectrometer and for the use of his lab space. S.E.D. would like to thank David M. Friday for starting this project and bringing it with him to UIUC.

Appendix A. Supplementary data

Supplementary data associated with this article can be found, in the online version, at http://dx.doi.org/10.1016/j.jms.2016.02.005. These data include MOL files and InChiKeys of the most important compounds described in this article.

References

[1] Demetre J. Economou, Pulsed plasma etching for semiconductor manufacturing, J. Phys. D – Appl. Phys. 47 (30) (2014).
[2] Hiroaki Kakiuchi, Hiromasa Ohmi, Kiyoshi Yasutake, Atmospheric-pressure low-temperature plasma processes for thin film deposition, J. Vac. Sci. Technol. A 32 (3) (2014).
[3] Mohammed Yousfi, Nofel Merbahi, Atul Pathak, Olivier Eichwald, Low-temperature plasmas at atmospheric pressure: toward new pharmaceutical treatments in medicine, Fundam. Clin. Pharmacol. 28 (2) (2014) 123–135.
[4] Gregory Fridman, Gary Friedman, Alexander Gutsol, Anatoly B. Shekhter, Victor N. Vasilets, Alexander Fridman, Applied plasma medicine, Plasma Process. Polym. 5 (6) (2008) 503–533.
[5] David B. Graves, Low temperature plasma biomedicine: a tutorial review, Phys. Plasmas 21 (8) (2014).
[6] G.B. McCombs, M.L. Darby, New discoveries and directions for medical, dental and dental hygiene research: low temperature atmospheric pressure plasma, Int. J. Dent. Hyg. 8 (1) (2010) 10–15.
[7] Gang Xiao, Weiping Xu, Rongbing Wu, Mingjiang Ni, Changming Du, Xiang Gao, Zhongyang Luo, Kefa Cen, Non-thermal plasmas for VOCs abatement, Plasma Chem. Plasma Process. 34 (5) (2014) 1033–1065.
[8] E. Tatarova, N. Bundaleska, J. Ph Sarrette, C.M. Ferreira, Plasmas for environmental issues: from hydrogen production to 2D materials assembly, Plasma Sources Sci. Technol. 23 (6) (2014).
[9] Ravindra B. Sabnis, Amit Bhattu, Vijaykumar Mohankumar, Sterilization of endoscopic instruments, Curr. Opin. Urol. 24 (2) (2014) 195–202.
[10] M. Moreau, N. Orange, M.G.J. Feuilloley, Non-thermal plasma technologies: new tools for bio-decontamination, Biotechnol. Adv. 26 (6) (2008) 610–617.
[11] M. Moisan, J. Barbeau, S. Moreau, J. Pelletier, M. Tabrizian, L.H. Yahia, Low-temperature sterilization using gas plasmas: a review of the experiments and an analysis of the inactivation mechanisms, Int. J. Pharmaceut. 226 (1–2) (2001) 1–21.
[12] Anne Mai-Prochnow, Anthony B. Murphy, Keith M. McLean, Michael G. Kong, Kostya (Ken) Ostrikov, Atmospheric pressure plasmas: infection control and bacterial responses, Int. J. Antimicrob. Agents 43 (6) (2014) 508–517.
[13] J. Ehlbeck, U. Schnabel, M. Polak, J. Winter, Th. von Woedtke, R. Brandenburg, T. von dem Hagen, K.-D. Weltmann, Low temperature atmospheric pressure plasma sources for microbial decontamination, J. Phys. D – Appl. Phys. 44 (1) (2011).
[14] Xue Zhang, Xiao-Fei Zhang, He-Ping Li, Li-Yan Wang, Chong Zhang, Xin-Hui Xing, Cheng-Yu Bao, Atmospheric and room temperature plasma (ARTP) as a new powerful mutagenesis tool, Appl. Microbiol. Biotechnol. 98 (12) (2014) 5387–5396.
[15] Rohit Thirumdas, Chaitanya Sarangapani, Uday S. Annapure, Cold plasma: a novel non-thermal technology for food processing, Food Biophys. 10 (1) (2015) 1–11.
[16] N.N. Misra, B.K. Tiwari, K.S.M.S. Raghavarao, P.J. Cullen, Nonthermal plasma inactivation of food-borne pathogens, Food Eng. Rev. 3 (3-4) (2011) 159–170.
[17] C. Meyer, S. Mueller, E.L. Gurevich, J. Franzke, Dielectric barrier discharges in analytical chemistry, Analyst 136 (12) (2011) 2427–2440.
[18] Jacob T. Shelley, Joshua S. Wiley, George C.Y. Chan, Gregory D. Schilling, Steven J. Ray, Gary M. Hieftje, Characterization of direct-current atmospheric-pressure discharges useful for ambient desorption/ionization mass spectrometry, J. Am. Soc. Mass Spectrom. 20 (5) (2009) 837–844.
[19] Anastasia Albert, Jacob T. Shelley, Carsten Engelhard, Plasma-based ambient desorption/ionization mass spectrometry: state-of-the-art in qualitative and quantitative analysis, Anal. Bioanal. Chem. 406 (25) (2014) 6111–6127.
[20] A.I. Egorov, S.I. Stepanov, Long-lived plasmoids produced in humid air as analogues of ball lightning, Tech. Phys. 47 (12) (2002) 1584–1586.
[21] Claire Tendero, Christelle Tixier, Pascal Tristant, Jean Desmaison, Philippe Leprince, Atmospheric pressure plasmas: a review, Spectrochim. Acta Part B: Atom. Spectrosc. 61 (1) (2006) 2–30.
[22] Noriyuki Hayashi, Hiroko Satomi, Toshinori Kajiwara, Tetsuo Tanabe, Properties of ball lightning generated by a pulsed discharge on surface of an electrolyte in the atmosphere, IEEJ Trans. Electr. Electron. Eng. 3 (6) (2008) 731–733.
[23] A. Versteegh, K. Behringer, U. Fantz, G. Fussmann, B. Jüttner, S. Noack, Long-living plasmoids from an atmospheric water discharge, Plasma Sources Sci. Technol. 17 (2) (2008) 024014.
[24] Youichi Sakawa, Kazuyoshi Sugiyama, Tetsuo Tanabe, Richard More, Fireball generation in a water discharge, Plasma Fusion Res. 1 (2006) (039-039).
[25] Karl D. Stephan, Shelby Dumas, Laurence Komala-Noor, Jonathan McMinn, Initiation, growth and plasma characteristics of "gatchina water plasmoids, Plasma Sources Sci. Technol. 22 (2) (2013) 025018.
[26] Scott E. Dubowsky, David M. Friday, Kevin C. Peters, Zhangji Zhao, Richard H. Perry, Benjamin J. McCall, Mass spectrometry of atmospheric-pressure ball plasmoids, Int. J. Mass Spectrom. 376 (0) (2015) 39–45.
[27] Pang Xuexia, Deng Zechao, Jia Pengying, Liang Weihua, Li Xia, Influence of ionization degrees on the evolutions of charged particles in atmospheric plasma at low altitude, Plasma Sci. Technol. 14 (8) (2012) 716.
[28] Yukinori Sakiyama, David B. Graves, Hung-Wen Chang, Tetsuji Shimizu, Gregor E. Morfill, Plasma chemistry model of surface microdischarge in humid air and dynamics of reactive neutral species, J. Phys. D: Appl. Phys. 45 (42) (2012) 425201.
[29] David M. Friday, Peter B. Broughton, Tanner A. Lee, Garrett A. Schutz, Jeremiah N. Betz, C. Michael Lindsay, Further insight into the nature of ball-lightning-like atmospheric pressure plasmoids, J. Phys. Chem. A 117 (39) (2013) 9931–9940.
[30] Jianyong Cen, Ping Yuan, Simin Xue, Observation of the optical and spectral characteristics of ball lightning, Phys. Rev. Lett. 112 (2014) 035001.
[31] John Abrahamson, Ball lightning from atmospheric discharges via metal nanosphere oxidation: from soils, wood or metals, Philos. Trans. Royal Soc. Lond. Ser. A: Math., Phys. Eng. Sci. 360 (1790) (2002) 61–88.
[32] Karl D. Stephan, Electrostatic charge bounds for ball lightning models, Phys. Scripta 77 (3) (2008) 035504.
[33] A.V. Shavlov, The two-temperature plasma model of a fireball. The calculated parameters, Phys. Lett. A 373 (43) (2009) 3959–3964.
[34] K. Tennakone, Stable spherically symmetric static charge separated configurations in the atmosphere: implications on ball lightning and earthquake lights, J. Electrostat. 69 (6) (2011) 638–640.

[35] S.V. Shevkunov, Cluster mechanism of the energy accumulation in a ball electric discharge, Doklady Phys. 46 (7) (2001) 467–472.
[36] L.S. Rothman, D. Jacquemart, A. Barbe, D. Chris Benner, M. Birk, L.R. Brown, M. R. Carleer, C. Chackerian Jr., K. Chance, L.H. Coudert, V. Dana, V.M. Devi, J.-M. Flaud, R.R. Gamache, A. Goldman, J.-M. Hartmann, K.W. Jucks, A.G. Maki, J.-Y. Mandin, S.T. Massie, J. Orphal, A. Perrin, C.P. Rinsland, M.A.H. Smith, J. Tennyson, R.N. Tolchenov, R.A. Toth, J. Van der Auwera, P. Varanasi, G. Wagner, The HITRAN 2004 molecular spectroscopic database, J. Quant. Spectrosc. Radiat. Transf. 96 (2) (2005) 139–204.
[37] C.M. Western, PGOPHER, A Program for Simulating Rotational Structure, University of Bristol. <http://pgopher.chm.bris.ac.uk>.
[38] Pierre-Franois Coheur, Peter F. Bernath, Michel Carleer, Reginald Colin, Oleg L. Polyansky, Nikolai F. Zobov, Sergei V. Shirin, Robert J. Barber, Jonathan Tennyson, A 3000k laboratory emission spectrum of water, J. Chem. Phys. 122 (7) (2005).
[39] C.C. Ferriso, C.B. Ludwig, L. Acton, Spectral-emissivity measurements of the 4.3-μ CO_2 band between 2650° and 3000°, J. Opt. Soc. Am. 56 (2) (1966) 171–173.
[40] K.P. Huber, G. Herzberg, Molecular Spectra and Molecular Structure: IV. Constants of Diatomic Molecules, Springer, US, 1979.
[41] H. Meinel, L. Krauss, ber die besetzung der rotationszustnde von oh und c2 in niederdruckplasmen, J. Quant. Spectrosc. Radiat. Transf. 9 (3) (1969) 443–460.
[42] C.I.M. Beenakker, F.J. De Heer, H.B. Krop, G.R. Mhlmann, Dissociative excitation of water by electron impact, Chem. Phys. 6 (3) (1974) 445–454.
[43] Jeffrey M. Headrick, Eric G. Diken, Richard S. Walters, Nathan I. Hammer, Richard A. Christie, Jun Cui, Evgeniy M. Myshakin, Michael A. Duncan, Mark A. Johnson, Kenneth D. Jordan, Spectral signatures of hydrated proton vibrations in water clusters, Science 308 (5729) (2005) 1765–1769.